Aerosol Science and Technology, 39:1–16, 2005

ISSN: 0278-6826 print / 1521-7388 online
DOI: 10.1080/027868290901891

The Reno Aerosol Optics Study: An Evaluation of Aerosol Absorption Measurement Methods

Patrick J. Sheridan,[1] W. Patrick Arnott,[2] John A. Ogren,[1] Elisabeth Andrews,[3] Dean B. Atkinson,[4] David S. Covert,[5] Hans Moosmüller,[2] Andreas Petzold,[6] Beat Schmid,[7] Anthony W. Strawa,[8] Ravi Varma,[2*] and Aki Virkkula[9]

[1]*Climate Monitoring and Diagnostics Laboratory, National Oceanic and Atmospheric Administration, Boulder, Colorado, USA*
[2]*Desert Research Institute, Reno, Nevada, USA*
[3]*Cooperative Institute for Research in Environmental Sciences (CIRES), University of Colorado, Boulder, Colorado, USA*
[4]*Department of Chemistry, Portland State University, Portland, Oregon, USA*
[5]*Department of Atmospheric Sciences, University of Washington, Seattle, Washington, USA*
[6]*Deutsches Zentrum fuer Luft- und Raumfahrt, Oberpfaffenhofen, Wessling, Germany*
[7]*Bay Area Environmental Research Institute, Sonoma, California, USA*
[8]*NASA Ames Research Center, Moffett Field, California, USA*
[9]*Finnish Meteorological Institute, Air Quality Research, Sahaajankatu, Helsinki, Finland*

The Reno Aerosol Optics Study (RAOS) was designed and conducted to compare the performance of many existing and new instruments for the in situ measurement of aerosol optical properties with a focus on the determination of aerosol light absorption. For this study, simple test aerosols of black and white particles were generated and combined in external mixtures under low relative humidity conditions and delivered to each measurement system. The aerosol mixing and delivery system was constantly monitored using particle counters and nephelometers to ensure that the same aerosol number concentration and amount reached the different instruments. The aerosol light-scattering measurements of four different nephelometers were compared, while the measurements of seven light-absorption instruments (5 filter based, 2 photoacoustic) were evaluated. Four methods for determining the aerosol light-extinction coefficient (3 cavity ring-down instruments and 1 folded-path optical extinction cell) were also included in the comparisons. An emphasis was placed on determining the representativeness of the filter-based light absorption methods, since these are used widely and because major corrections to the raw attenuation measurements are known to be required. The extinction measurement from the optical extinction cell was compared with the scattering measurement from a high-sensitivity integrating nephelometer on fine, nonabsorbing ammonium sulfate aerosols, and the two were found to agree closely (within 1% for blue and green wavelengths and 2% for red). The wavelength dependence of light absorption for small kerosene and diesel soot particles was found to be very near λ^{-1}, the theoretical small-particle limit. Larger, irregularly shaped graphite particles showed widely variable wavelength dependencies over several graphite runs. The light-absorption efficiency at a wavelength of 530 nm for pure kerosene soot with a number size distribution peak near 0.3 μm diameter was found to be 7.5 $\pm$ 1.2 m^2 g^{-1}. The two most fundamental independent absorption methods used in this study were photoacoustic absorption and the difference between suspended-state light extinction and scattering, and these showed excellent agreement (typically within a few percent) on mixed black/white aerosols, with the photoacoustic measurement generally slightly lower. Excellent agreement was also observed between some filter-based light-absorption measurements and the RAOS reference absorption method. For atmospherically relevant levels of the aerosol light-absorption coefficient ($<$25 Mm^{-1}), the particle soot absorption photometer (PSAP) absorption measurement at mid-visible wavelengths agreed with the reference absorption measurement to within $\sim$11% for experiment tests on externally mixed kerosene soot and ammonium sulfate. At higher absorption levels (characterized by lower single-scattering albedo aerosol tests), this agreement worsened considerably, most likely due to an inadequate filter loading correction used for the PSAP. The PSAP manufacturer's filter loading correction appears to do an adequate job of correcting the PSAP absorption measurement at aerosol single-scattering albedos above 0.80–0.85, which represents

Received 29 January 2004; accepted 22 October 2004.
We gratefully acknowledge encouragement and funding support from the NOAA Office of Global Programs, Aerosol-Climate Interactions Program and the DOE Atmospheric Radiation Measurement Program.
*Present address: Arcadis, Inc., P. O. Box 13109, Research Triangle Park, NC 27709.
Address correspondence to Patrick J. Sheridan, Climate Monitoring and Diagnostics Laboratory, National Oceanic and Atmospheric Administration, 325 Broadway, Boulder, CO 80305, USA. E-mail: patrick.sheridan@noaa.gov

most atmospheric aerosols, but it does a progressively worse job at lower single-scattering albedos. A new filter-based light-absorption photometer was also evaluated in RAOS, the multiangle absorption photometer (MAAP), which uses a two-stream radiative transfer model to determine the filter and aerosol scattering effects for a better calculation of the absorption coefficient. The MAAP absorption measurements agreed with the reference absorption measurements closely (linear regression slope of ~0.99) for all experimental tests on externally mixed kerosene soot and ammonium sulfate.

INTRODUCTION

It is now widely accepted that aerosols have the potential to perturb the radiation balance of the planet either directly through scattering and absorption of solar radiation or indirectly by altering cloud properties. These aerosol-induced changes in radiative fluxes are referred to as aerosol radiative forcing, the importance of which as a component of climate forcing has recently begun to be understood (e.g., Coakley and Cess 1985; Charlson et al. 1991; IPCC 1995, 2001; Hansen et al. 1997; Rosenfeld 2000). Several recent field experiments including SCAR-B (Kaufman et al. 1998), TARFOX (Russell et al. 1999), LACE 98 (Ansmann et al. 2002), and INDOEX (Ramanathan et al. 2001) have been conducted with the objective of reducing the uncertainties in predicting climate change due to aerosol effects. These studies have shown the magnitude of the aerosol forcing to be quite large at times downwind of major aerosol source regions. While these field experiments provided valuable information on the optical properties of ambient aerosols and multiple instrument intercomparison approaches, the studied aerosols could not be systematically varied with respect to composition, size distribution, mixing state, etc., to better understand how these factors affect the measurement and associated uncertainty of aerosol optical properties.

In order to reduce the uncertainties in our estimates of aerosol radiative forcing, better measurements of aerosol optical properties must be made. Currently, aerosol light absorption measurements typically show larger and more poorly understood uncertainties than do extinction and scattering measurements. Aerosol light absorption measurements are important for quantifying the role of black carbon (BC) aerosol, the dominant atmospheric aerosol light-absorbing species, in climate change. The strong impact of the absorbing component on the forcing for a continental aerosol and a forest fire layer in the free troposphere has been demonstrated by Petzold et al. (2002). Improvement in our ability to measure light absorption by atmospheric aerosols should reduce the uncertainty in our estimates of the aerosol single-scattering albedo (ϖ_0), a key aerosol property needed for radiative forcing calculations.

Few fundamental laboratory studies have been conducted to assess the state-of-the-art in aerosol optical property measurement by comparing the popular methodologies. The most comprehensive study found in the literature is the First International Workshop on Light Absorption by Aerosol Particles (Gerber 1982a) held at Colorado State University during summer 1980. In this study, presumably identical, well-characterized aerosol mixtures were provided to a large number of participants to measure by a variety of techniques. The current state-of-the-art of in situ aerosol absorption, scattering, and extinction instruments were represented, and aerosol characterization measurements such as size distribution, chemistry, and mass were also made. At the time of this study, all methods for measuring light absorption by aerosol particles were found to have potentially large errors, which were estimated to be on the order of a factor of two or three in the visible (Gerber 1982b). These errors were, however, considerably smaller than the natural variability of aerosol light absorption in the atmosphere, so useful measurements could be made at that time.

A recent international soot aerosol characterization experiment was conducted in 1999 at the AIDA aerosol chamber in Karlsruhe, Germany (Saathoff et al. 2003a). In this experiment, the optical, chemical, and microphysical properties of soot aerosols were studied using many techniques, with a major objective being to compare soot from a diesel vehicle with artificial soot from a spark generator. External mixtures of soot and ammonium sulfate particles were investigated, as were soot particles with organic coatings (Saathoff et al. 2003b). One of the findings from this experiment was that many characteristics of the artificial soot, including morphology, spin density, and mass specific extinction cross section, were significantly different from those of the diesel soot aerosols.

In this article, we give an overview and discuss the major results of a recent laboratory study designed to compare numerous instruments that measure atmospheric aerosol optical properties. During 3–28 June 2002, the Reno Aerosol Optics Study (RAOS) was conducted at the Desert Research Institute in Reno, Nevada, USA. The objective was to characterize, under controlled laboratory conditions, both existing and new instruments designed to measure in situ aerosol light extinction, scattering, and absorption, with a focus on evaluating the accuracy of and agreement between absorption methods. In some respects, this study is similar to Gerber (1982a) and Saathoff et al. (2003a). However, substantial improvements over the years in instrument sensitivity and performance, and a number of new instruments, call for a study of this type to be performed again. Included in the RAOS experiment were three cavity ring-down extinction instruments, one classic folded-path optical extinction cell (OEC), four integrating nephelometers, two photoacoustic absorption instruments, and five filter-based absorption instruments, as well as numerous other instruments and methods for aerosol microphysical and chemical characterization. Good coverage of the visible spectrum was achieved from the operating wavelengths of the various instruments, with limited measurements made in the near UV and near IR.

The RAOS emphasis on absorption was necessary to evaluate the accuracy and precision of current methods for measuring the atmospheric aerosol light-absorption coefficient (σ_{ap}). We were particularly interested in understanding the factors

responsible for and quantifying the uncertainty in the filter-based measurements of σ_{ap} made around the world by the National Oceanic and Atmospheric Administration's (NOAA) Climate Monitoring and Diagnostics Laboratory (CMDL) and the Department of Energy's (DOE) Atmospheric Radiation Measurement (ARM) program. From this study, we also hoped to derive methods for calculating spectral aerosol absorption from multiwavelength measurements of absorption. While some of the major results from RAOS are presented herein, this article serves as an introduction for several other RAOS papers (e.g., Arnott et al. 2005; Petzold et al. 2005; Virkkula et al. 2005a, b) in which detailed results and discussions of the individual instruments and measurements are offered.

EXPERIMENTAL METHODS

The RAOS was conducted during 3–28 June, 2002 in the Optics and Acoustics Laboratory of the Desert Research Institute (DRI) in Reno, NV. During the first week, prior to any instrument intercomparison tests, aerosol generation, characterization, and delivery issues were investigated and optimized. A schematic of the aerosol generation and delivery system as configured for most of the experiment is shown in Figure 1. This arrangement was used whenever particles from a soot-producing kerosene lamp were used as the standard "black" aerosol. Two other types of black aerosols were tested during the study; these were particles from a diesel generator parked outside the building and the exhaust particles from a graphite vane pump.

Since all of the participating light absorption instruments were very sensitive to black carbon aerosols, an eductor system was fabricated to dilute the black aerosols with filtered air by up to 2 orders of magnitude. A particle-free compressed air source was used for this dilution with an additional HEPA filter in line. Variation of the ratio of filtered air to soot aerosol flow permitted fine control of the amount of black aerosols entering the main aerosol mixing chamber.

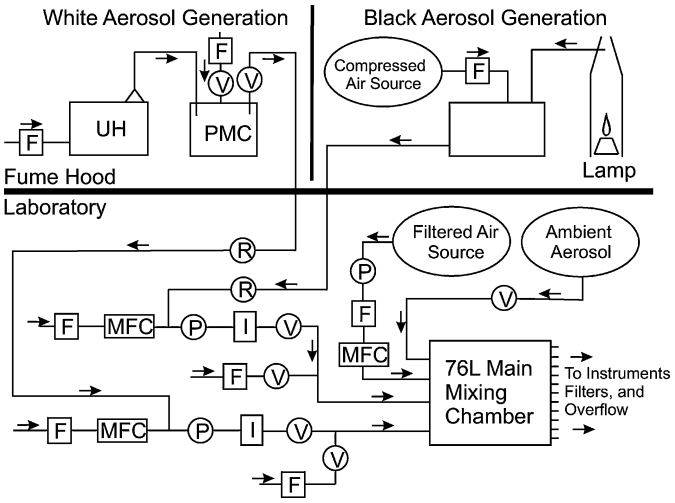

Figure 1. Schematic of the RAOS aerosol generation and delivery system. Generation of white and black aerosols took place in the fume hood, and arrows indicate direction of air/aerosol flow. In this diagram, F = HEPA filter, V = ball valve, I = 1-μm cutpoint impactor, R = rotameter, P = diaphragm pump, UH = ultrasonic humidifier, MFC = mass flow controller, and PMC = 10 l preliminary mixing/drying chamber.

White aerosols used in most of the intercomparisons were ammonium sulfate generated with an ultrasonic humidifier (UH). Source air for the UH was filtered, and the output was directed into a preliminary mixing/drying chamber (PMC), where significant drying of the wet $(NH_4)_2SO_4$ aerosols occurred. Dry-filtered laboratory air was pulled into the PMC as necessary for the mixing and drying to occur.

Separate diaphragm pumps were used to transfer the black and white aerosols (and filtered air) into the large (76 l), stainless steel main mixing chamber (MMC). These aerosol transfer pumps were used to keep the MMC and sampling lines at a slight positive pressure (a few mb above laboratory pressure) so that potential leaks in the aerosol mixing and delivery system would not be a problem. One outlet port on the MMC was used as an overflow port, and flow out of the chamber was visually verified using a rotameter. Pressure inside the vessel was continuously monitored using an MKS Barotron sensor, and MMC temperature and relative humidity (RH) were measured using a Vaisala humitter probe. Typical RHs inside the mixing vessel were low and ranged between 15–25%. This last point requires emphasis; the results presented in this article are representative of low RH conditions and therefore may not represent atmospheric aerosols at all places and times. The low and consistent test RHs should, however, minimize variability in the aerosol optical properties due to changing humidities (Covert et al. 1972; Rood et al. 1987; Redemann et al. 2001), thus permitting a better observation of the optical properties in multiple instruments.

The MMC had four closely positioned inlet ports on one side of the vessel; these were for introducing white aerosols, black aerosols, ambient (outdoor) aerosols, and filtered air. Black and white test aerosols were passed through identical 1 μm aerodynamic diameter cutpoint impactors, which were treated with silicone grease to minimize particle bounce. An aerodynamic diameter of 1 μm is equivalent to a geometric diameter of $\sim$0.75 μm for $(NH_4)_2SO_4$ particles, so the actual size distributions of $(NH_4)_2SO_4$ test aerosols in this study show an upper-limit truncation at $\sim$0.75 μm diameter. Due to the aggregate nature of soot particles, it is difficult to know the true size of the soot aggregates that passed the impactors, but the primary spherules comprising these aggregates were found to be consistently 20–50 nm in size.

Some aerosol losses were observed in the aerosol transfer pumps, so it was decided that ambient aerosols would be drawn into the chamber using the pumps from the participating instruments. While this introduced the possibility of leaks of laboratory air during the ambient aerosol runs, no leaks were observed when operating at the pressure drops used in the tests. Ambient aerosols were sampled using a 1.91 cm outer diameter (o.d.)

copper tube inserted through the laboratory wall. Sampling was at ~10 m above the surface above one wing of the main DRI building. Parking lots were nearby, and a busy highway was within 1 km of the inlet.

A small fan mixed the aerosols from the inlet ports as they entered the MMC. A stainless steel baffle bisected the chamber from top to bottom, separating the inlet and outlet sides of the vessel. The only way for aerosols to get from the inlet to the outlet side was for them to go around or through the perforated baffle. Based on sample port tests conducted prior to and during the RAOS (described below), this process appeared to mix the aerosols thoroughly in transit to the outlet ports.

The size of the test aerosols was monitored using a TSI scanning mobility particle sizer (SMPS), sensitive to particles in the size range 0.012–0.6 μm diameter. For the white aerosols, the amount of $(NH_4)_2SO_4$ in solution in the UH was adjusted to achieve a number size peak in the 0.2–0.3 μm diameter range. It was difficult to control the soot size distributions (without significantly affecting other things such as particle number and NO_x generation), so we just used what the generators produced. Figure 2 shows typical size distributions from the SMPS

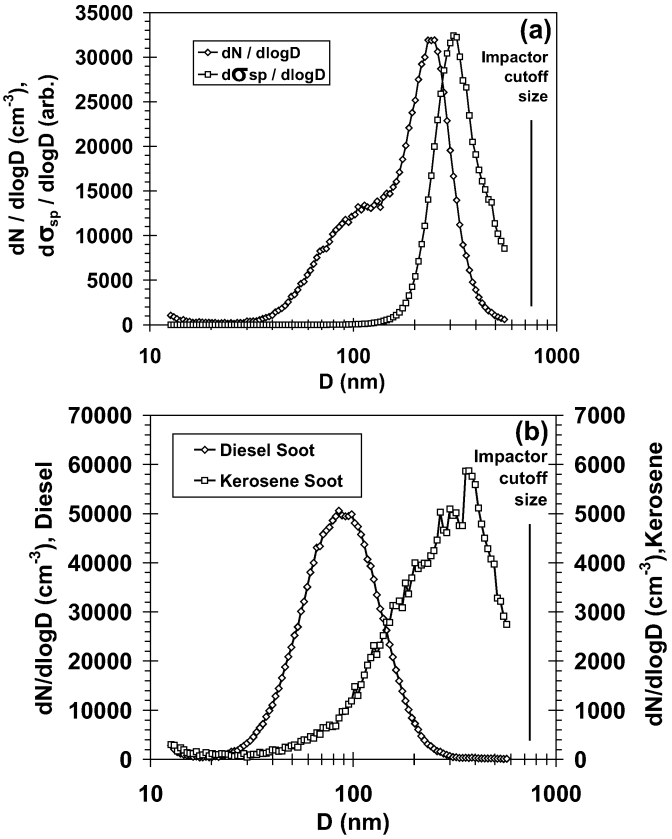

Figure 2. (a) Typical $(NH_4)_2SO_4$ aerosol number and scattering size distributions for a high-extinction (~500 Mm^{-1}) run. The 1 μm aerodynamic-diameter cutpoint impactors produced an actual physical cutpoint of approximately 0.75 μm diameter. (b) Typical diesel and kerosene soot number size distributions.

obtained during one high-extinction (~500 Mm^{-1}) $(NH_4)_2SO_4$ and two soot aerosol runs. The $(NH_4)_2SO_4$ number size distribution in Figure 2a appears slightly bimodal, although virtually all of the scattering is from the larger particle mode. It is important to note that most of the actual size distribution is accounted for in the SMPS data. Only the particles between ~0.6 and 0.75 μm would have passed the impactor but not been measured by the SMPS. The shape of the measured size distribution suggests that very little aerosol scattering was missed in the SMPS calculations. We operated the diesel generator under high engine load conditions, and the diesel particle size distribution depends significantly on engine loading (e.g., Panne et al. 1995; Kittleson 1998). The kerosene soot showed a broader size distribution and significantly fewer particles than the diesel soot.

The outlet wall of the MMC contained 18 equally spaced ports, made from 1/2-inch Swagelok bulkhead connectors. Tests were run on ammonium sulfate aerosols using multiple TSI 3010 condensation particle counters (CPCs) and TSI 3563 integrating nephelometers during the first week of the experiment (before the instrument intercomparisons) to ensure that the same aerosol concentration (determined by aerosol number and scattering coefficient) was transferred to each port. Tests were repeated with the positions of CPCs and nephelometers reversed to account for instrument measurement differences. Differences in aerosol numbers between all ports were small, typically $<1\%$ and never above 2%. Scattering coefficients measured from different ports on the MMC were typically within 2% of one another.

In addition to the SMPS, several other methods were used throughout the duration of the RAOS to characterize and monitor the type and amount of aerosols in the system. Table 1 shows the methods utilized for aerosol characterization during the RAOS. Three TSI Model 3010 and one TSI Model 3025 CPCs were used to monitor aerosol number concentration continuously at different points in the aerosol mixing and delivery system. A tapered element oscillating microbalance (TEOM; Rupprecht and Patashnick, Inc.) continuously measured aerosol mass concentration in the MMC to ensure consistency of the source aerosol. Aerosol filter samplers attached to two sampling ports of the MMC, one containing a quartz fiber filter and one containing a membrane filter, were used to collect particles for subsequent elemental carbon/organic carbon (EC/OC) determination (Chow et al. 1993) and electron microscopy analysis, respectively. A photomicrograph of the mixed ammonium sulfate/kerosene soot aerosols is shown in Figure 3. As is evident in the image, the two aerosol types were predominantly externally mixed. The $(NH_4)_2SO_4$ particles were roughly spherical, simplifying calculation of the expected scattering using Mie code, and the SMPS number peak at 0.2–0.3 μm diameter was corroborated through the microscopy analyses.

All aerosol delivery lines between the MMC and instruments were 1.27 cm o.d. copper tubing, with gentle bends and similar lengths to the extent possible. After the arrangement of instruments around the MMC was finalized, tests with CPCs and nephelometers positioned at the ends of the sampling lines

Table 1
Aerosol characterization measurements performed during RAOS

Measurement	Method	Detection limit
Aerosol size distribution	TSI 3025/3071-based SMPS	$0.012 < D_p < 0.6$ μm diameter
Aerosol number concentration	TSI 3010 (and 3025) CPCs	0.01 (0.003) μm $< D_p < 1$ μm diameter
Aerosol mass concentration	TEOM	10 μg m^{-3}
Carbonaceous composition	EC/OC analysis of quartz filters by thermal/optical reflectance method*	EC: 0.0–0.2 μg C cm^{-2}* OC: 0.5–1.0 μg C cm^{-2}*
Particle morphology	SEM analysis of membrane filters	$D_p > \sim$10 nm diameter

*From Chow et al. (1993).

were conducted to ensure that the same amount of aerosols was transmitted through the different lines. The results were similar to those obtained from the sampling port tests, indicating that aerosol transmission efficiencies were the same. After the start of the instrument intercomparisons, the positions of CPCs were moved periodically to compare different sampling lines. There was no evidence of an uneven distribution of aerosols to the instruments.

The experimental matrix used for the creation of target aerosol mixtures is shown in Table 2. An attempt was made to generate aerosols with widely varying extinction levels and covering a large range of single-scattering albedos in the mid-visible range. The target extinctions and single-scattering albedos were achieved and maintained by monitoring scattering and absorption coefficients reported by an integrating nephelometer and a photoacoustic spectrometer. If, for example, the extinction or the single-scattering albedo drifted from its target value, minor manual adjustments in the amount of white or black aerosols or filtered air entering the MMC could be made in real time to adjust the mixture back to the target.

Three extinction ranges were used: Low (0–100 Mm^{-1}), Medium (100–300 Mm^{-1}), and High (300–600 Mm^{-1}). The range of single-scattering albedos covered was 1.0 for unmixed ammonium sulfate aerosols to ~0.3 for unmixed black kerosene and diesel soot. Time constraints eliminated the possibility of testing many aerosol mixtures at all target extinction levels and single-scattering albedos. The first priority was to provide mixtures of $(NH_4)_2SO_4$ and kerosene soot over all targeted extinction ranges and single-scattering albedos. The next priority was to generate mixtures with different black aerosols (e.g., either graphite particles or diesel soot) and measure their optical properties to see how they differed from the kerosene soot tests. This was done in a limited fashion for graphite particles at the medium extinction. The two different diesel generators that were used generated so much NO_x along with the soot particles that

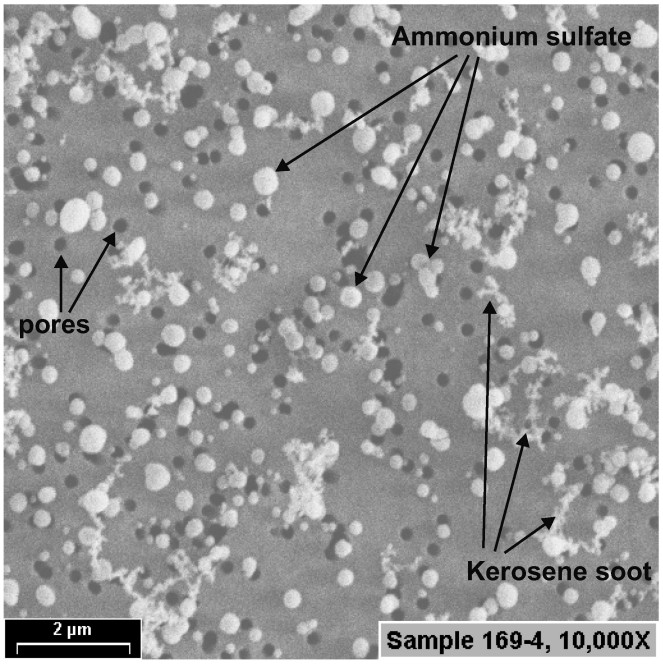

Figure 3. Externally mixed $(NH_4)_2SO_4$ and kerosene soot aerosols collected during one of the RAOS sampling runs. Collection substrate was 0.2 μm pore size membrane filter.

Table 2
Experimental target matrix for conducting aerosol optical property instrument intercomparison tests

	σ_e (Mm^{-1})		
ϖ_0	Low (5–100)	Medium (100–300)	High (300–600)
1.00	AS	AS	AS
0.98	AS + K	AS + K, AS + G	AS + K
0.95	AS + K	AS + K, AS + G	AS + K
0.90	AS + K	AS + K, AS + G	AS + K
0.80	AS + K	AS + K, AS + G	AS + K
0.70	AS + K	AS + K, AS + G	AS + K
All black	K, D, G	K	K
Other	A, F, PSL		PSL

White aerosols: ammonium sulfate (AS).
Black aerosols: kerosene soot (K), diesel soot (D), graphite (G).
Other: ambient air (A), filtered air (F), polystyrene latex 0.5 μm diameter (PSL).

NO_2 denuders were quickly saturated and gas-phase absorption was a dominant interference in the measurements. Therefore, we have only one valid diesel soot run at a low extinction level. In addition to the aforementioned aerosol mixtures, other measurements on filtered air, ambient aerosols, and polystyrene latex spheres (0.5 μm diameter) were made.

Table 3 shows a list of the measurements, instruments, operating wavelengths, and institutions participating in the RAOS. Measurements of the aerosol light-absorption coefficient (σ_{ap}) were made using two primary methods, which were photoacoustic spectroscopy and the difference between aerosol light extinction and light scattering ($\sigma_{ep} - \sigma_{sp}$). In addition, several filter-based light-attenuation measurements were made from which σ_{ap} was derived. The two most common commercially available, filter-based light-absorption instruments were represented in this study. Two seven-wavelength aethalometers (Magee Scientific Model AE-8) and two particle soot absorption photometers (Radiance Research Model PSAP) were used to derive σ_{ap} (Arnott et al. 2005). One of the aethalometers had three of the source LEDs replaced so that different regions of the visible spectrum were covered. One of the PSAPs was modified to operate at three wavelengths, with these wavelengths matching

Table 3
Aerosol optical property measurements and instruments in the RAOS

Measurement	Method	Instrument	Operating wavelengths	Institution
Aerosol light absorption coefficient, σ_{ap}	Photoacoustic absorption	Photoacoustic spectrometer	532 nm	Desert Research Institute
σ_{ap}	Photoacoustic absorption	Photoacoustic spectrometer	1047 nm	Desert Research Institute
σ_{ap}	Filter-based absorption	PSAP*	565 nm	NOAA/CMDL
σ_{ap}	Filter-based absorption	3 wavelength PSAP	467, 530, 660 nm	University of Washington
σ_{ap}	Filter-based absorption	7 wavelength Aethalometer	370, 470, 521, 590, 660, 880, 950 nm	Desert Research Institute
σ_{ap}	Filter-based absorption	7 wavelength Aethalometer	370, 430, 470, 521, 565, 700, 950 nm	NOAA/CMDL
σ_{ap}	Filter-based absorption	Carusso	670 nm	ThermoESM Anderson
σ_{ap}	In situ absorption (by difference)	Cavity ring-down instrument	690 nm	NASA/ARC
σ_{ap}	In situ absorption (by difference)	Optical extinction cell and integrating nephelometer	467, 530, 660 nm	Univ. of Washington and NOAA/CMDL
Aerosol light scattering coefficient, σ_{sp}	Integrating nephelometry	TSI 3563 integrating nephelometer	450, 550, 700 nm	NOAA/CMDL
σ_{sp}	Integrating nephelometry	Radiance Research M903 integrating nephelometer	530 nm	Desert Research Institute
σ_{sp}	Integrating nephelometry	DRI integrating sphere nephelometer	532 nm	Desert Research Institute
σ_{sp}	Integrating nephelometry	NASA/Ames CRD nephelometer	690 nm	NASA/ARC
Aerosol light extinction coefficient, σ_{ep}	Aerosol extinction	Folded-path optical extinction cell	467, 530, 660 nm	University of Washington
σ_{ep}	Aerosol extinction	Cavity ring-down instrument	532 nm	Desert Research Institute
σ_{ep}	Aerosol extinction	Cavity ring-down instrument	532, 1064 nm	Portland State University
σ_{ep}	Aerosol extinction	Cavity ring-down instrument	690, 1550 nm	NASA/ARC

*565 nm is the manufacturer's stated operating wavelength.

those of a folded-path OEC. A third type of filter-based light-absorption instrument, called multiangle absorption photometer (MAAP; ThermoESM/Anderson), was also compared in this study (Petzold and Schönlinner 2004). This new light-absorption photometer not only measures the attenuation of transmitted light through the filter with increasing particle loading (as do the aethalometer and PSAP), it also measures the reflectance of the front face of the filter at different angles to obtain a better estimate of the multiple scattering effects of aerosols and filter medium. A two-stream radiative transfer model is then used to derive the aerosol absorption coefficient, accounting for light scattered by both particles and filter. The MAAP has a detection limit of $\sim$1 Mm^{-1} for 2 min average data at a flow rate of 16.7 l min^{-1}.

Measurements of the aerosol light-scattering coefficient (σ_{sp}) were made using two commercially available integrating nephelometers (3-wavelength TSI Model 3563 and single-wavelength Radiance Research Model M903). A third scattering measurement was available using the DRI integrating sphere nephelometer (Varma et al. 2003). This nephelometer operates at 532 nm and integrates light scattering from particles over an angle approaching 180°, so it was expected to have very small truncation errors associated with its measurement. Another instrument, which is described below, also measured σ_{sp} and gave us a total of four independent scattering measurements in the RAOS.

The aerosol light-extinction coefficient (σ_{ep}) was measured using a classic folded-path OEC (Virkkula et al. 2005a) and three newly developed cavity ring-down (CRD) instruments (Smith and Atkinson 2001; Strawa et al. 2003; Moosmüller et al. 2005). The OEC has a total optical path length of $\sim$6.6 m and measures extinction at 467, 530, and 660 nm. The difference between the σ_{ep} measurement from the OEC and the σ_{sp} measurement from the TSI nephelometer (after correction for angular nonidealities in the nephelometer (Anderson and Ogren 1998) and adjustment to a common wavelength) was used for the (extinction–scattering) σ_{ap} determination. When comparing other absorption methods with the ($\sigma_{ep} - \sigma_{sp}$) absorption, only tests where the OEC σ_{ep} was >50 Mm^{-1} were used so that extinction cell noise would not dominate the extinction–scattering determination.

The three CRD instruments participating in RAOS employed different measurement strategies. The Portland State University (PSU) instrument used a pulsed Nd-YAG laser at 532 and 1064 nm (Smith and Atkinson 2001). In this instrument, the aerosol flow and optical axes were collinear. The aerosol flow (3.0 l min^{-1}) entered the center of the ring-down cell and exited at the ends. A small ($\sim$0.3 l min^{-1}) purge flow was introduced to the ends of the cavity to keep the mirrors clean. This resulted in an effective particle-laden optical path length of 0.75 ± 0.05 m, where the stated uncertainty is intended to reflect the nonideal containment of the aerosol flow. The DRI instrument also used a pulsed Nd-YAG laser at 532 nm with aerosol flow along the optical axis. The laser on this instrument was chopped at 15 Hz, allowing cavity-enhanced detection analysis to be performed simultaneously with standard ring-down analysis. The aerosol flow entered at one end of the cell and exited at the opposite end. A small purge flow was introduced to keep the mirrors clean in this instrument also. The NASA Cadenza CRD instrument employed a continuous wave (CW-CRD) technique at 690 and 1550 nm (Strawa et al. 2003). In this instrument the aerosol flow was perpendicular to the optical axis and clean purge flows formed an aerodynamic window to keep the mirrors clean and define the length of the aerosol-laden flow in the ring-down cell. Scattered light at 690 nm was collected simultaneously by a diffuser and photomultiplier combination mounted on the ring-down cell for simultaneous measurement of scattering and extinction coefficients, giving this instrument the capability to determine by difference the light-absorption coefficient and the single-scattering albedo.

Aerosol optical properties and concentration, along with vessel pressure, temperature, and RH were continuously monitored in the MMC during instrument intercomparison runs to guard against rapidly changing conditions. Scattering coefficients at 550 nm from the TSI 3563 nephelometer and absorption coefficients from the 565 nm PSAP, corrected to 550 nm using the Bond et al. (1999) (hereafter referred to as B1999) method, were used for these real-time observations of aerosol variability. Figure 4 shows optical property data from a relatively stable 84 min $(NH_4)_2SO_4$ aerosol run. In this figure, time is expressed in Day of the Year (DOY). In this run, the σ_{sp} at 550 nm varied slowly over a range of $\sim$130–150 Mm^{-1} for most of the run (Figure 4a). The calculated single-scattering albedo, as shown in Figure 4b, varied from $\sim$0.986 to 0.993 during this period. Stability of this order was typical for about one-half of all aerosol runs, and in cases like these data from the entire run were used.

The rest of the runs showed larger aerosol variability. An example of this is shown in Figure 5. The first half of the aerosol run was relatively stable, as shown in Figure 5a. At around DOY 168.897, the black aerosol generation system became unstable and more kerosene soot was introduced into the mixing chamber. Figure 5b shows the large drop in aerosol single-scattering albedo at this time. Adjustment of the flame and aerosol flows returned the black aerosol to its previous levels, but a large spike and decay is evident in the measurements. In runs such as these, where the aerosol concentrations were not stable, a "subrun" was defined that included only the most stable portion of the run. The elimination of the variable aerosol period minimizes potential differences in the measurements caused by different flow rates and/or residence times among the various instruments. In this run, the period from DOY 168.878 to 168.895 was defined as a subrun, as shown in the Figures 5a and 5b.

RESULTS AND DISCUSSION

Since the RAOS was an experiment focused on the determination of how well we can measure aerosol light absorption, a question arose during the study as to which technique(s) should be our "reference" for aerosol light absorption, against which

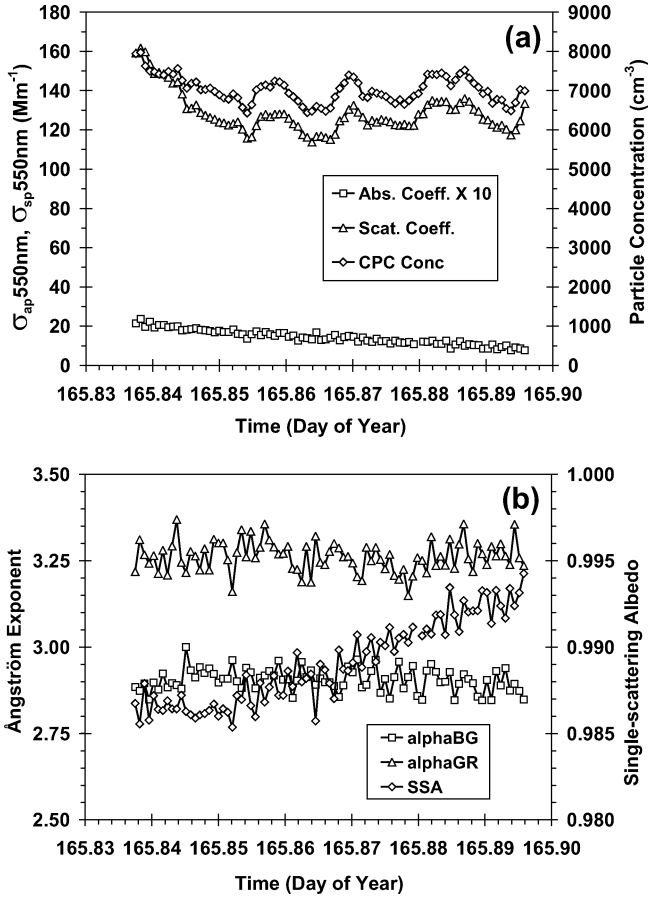

Figure 4. (a) Light-scattering coefficient (550 nm), light-absorption coefficient (550 nm), and CPC particle concentration (cm^{-3}) for a relatively stable aerosol run. (b) Ångström exponents (450/550 nm and 550/700 nm) and single-scattering albedo for this aerosol run.

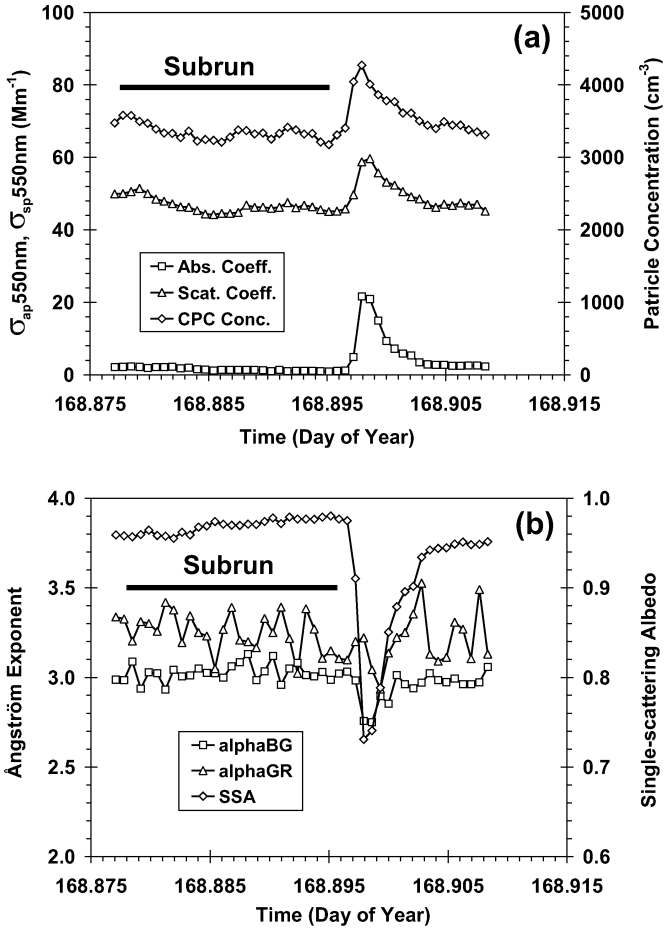

Figure 5. (a) Light-scattering coefficient (550 nm), light-absorption coefficient (550 nm), and CPC particle concentration (cm^{-3}) for an unstable aerosol run. An increase in black aerosol output occurred starting at Day 168.897. (b) Ångström exponents (450/550 nm and 550/700 nm) and single-scattering albedo for this aerosol run. Portion of experiment used for instrument comparison is marked as "Subrun" in both plots.

other measurements would be judged. It is clear that the commonly used filter methods suffer from major artifacts associated with the multiple-scattering filter medium and scattering aerosols deposited on the filter surface (e.g., B1999). The new MAAP instrument was said to treat these interferences (Petzold and Schönlinner 2004), but at the time of the RAOS it had not undergone rigorous comparisons with other techniques. The photoacoustic method has been touted as the preferred way to measure atmospheric aerosol light absorption, because there are no filter artifacts and because it does not respond appreciably to scattering aerosols (Andreae 2001). Another robust method to obtain aerosol light absorption is to measure independently both extinction and scattering on suspended particles and calculate the difference (Gerber 1982b; Horvath 1993). This method has been used numerous times in the past for atmospheric measurements and was in fact used to calibrate the PSAP (B1999). Both the photacoustic and the "extinction minus scattering" absorption methods are traceable to independent calibrations for which standards exist. These utilize the photoacoustic spectrometer (NO_2 absorption), the nephelometers (CO_2 scattering), and the long-path extinction cell (meter stick). Since we had no way of knowing a priori which of these two methods was superior, we decided that our "reference" absorption coefficient ($\sigma_{ap(REF)}$) for this study was the average of the 532 nm photoacoustic measurement (adjusted to 530 nm) and the difference of OEC extinction and truncation-corrected TSI nephelometer scattering ($\sigma_{ep} - \sigma_{sp}$), adjusted to the common wavelength of 530 nm by log-interpolation. As implied above, only tests where the OEC σ_{ep} was >50 Mm^{-1} were used for calculating reference absorption.

In order to confirm that the OEC and nephelometer could yield a valid difference measurement for absorption on mixed aerosols, a test on laboratory-generated nonabsorbing $(NH_4)_2SO_4$ aerosols was conducted. The imaginary refractive index of $(NH_4)_2SO_4$ in the mid-visible spectrum is very close

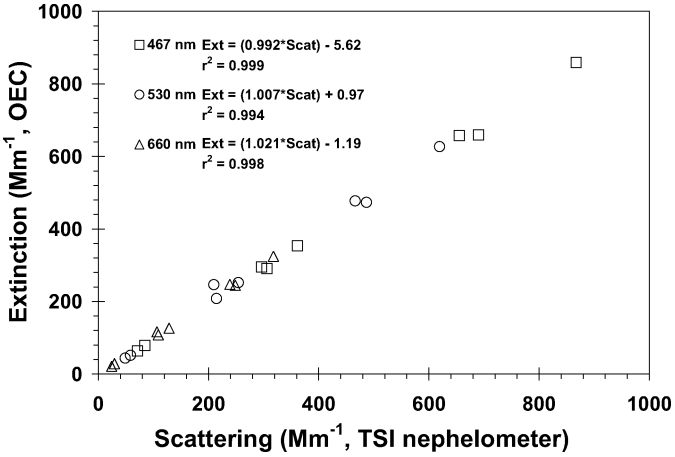

Figure 6. Comparison of concurrent extinction measurements from the University of Washington's OEC with scattering measurements from the NOAA TSI 3563 nephelometer for white (pure $(NH_4)_2SO_4$) aerosol runs.

to zero (Toon et al. 1976); thus light absorption by this aerosol should be negligible and the extinction and scattering measurements should agree closely. Figure 6 shows a comparison of the extinction and scattering measurements on this aerosol. The 24 data points in this plot represent all 8 of the test runs for which both the University of Washington OEC and the NOAA TSI 3563 nephelometer were measuring $(NH_4)_2SO_4$ aerosols at three wavelengths. The scattering coefficients from the TSI nephelometer were corrected for angular nonidealities using the methods of Anderson and Ogren (1998). Nephelometer wavelengths were adjusted to match the OEC wavelengths through log-interpolation using the Ångström exponent. The results show that extinction and scattering measurements from these two instruments on white aerosols agree to within ~2% at 660 nm and to better than 1% in the green and blue channels (530 and 467 nm, respectively). A detailed discussion of the uncertainties inherent in the $(\sigma_{ep} - \sigma_{sp})$ reference absorption method can be found in B1999.

As shown in Table 3, many of the instruments that measured σ_{ap} in this experiment operated at different wavelengths. In order to compare two measurements at different wavelengths, the wavelength dependence of light absorption must be known or assumed so that a wavelength adjustment can be done for at least one of the measurements. This determination is difficult to make for internally mixed black carbon (BC) particles, especially those with a solid black core and a surrounding or attached liquid phase, because the mass absorption efficiency is a function of both particle size and wavelength (Ackerman and Toon 1981; Fuller et al. 1999; Redemann et al. 2001). It has been shown that for small, spherical absorbing particles of constant refractive index (particle diameter, D_p, $< \sim 0.02\ \mu$m at $\lambda = 550$ nm) the absorption per unit mass is independent of size and the wavelength dependence is λ^{-1} (i.e., the theoretical "small particle limit") (van de Hulst 1957; Bergstrom 1973; Bohren and Huffman 1983). It has been estimated that the wavelength dependence of the absorption coefficient of small spherical atmospheric BC particles with constant indices of refraction should be $\sim\lambda^{-1}$ to $\lambda^{-1.3}$ or less (Bergstrom et al. 2002). RAOS measurements of σ_{ap} on kerosene and diesel soot aerosols from both of the photoacoustic instruments and the $(\sigma_{ep} - \sigma_{sp})$ method suggest an $\sim\lambda^{-1}$ dependence for aerosol light absorption over the visible range. Figure 7 shows typical (extinction–scattering) σ_{ap} determinations at 3 visible wavelengths, with the scattering coefficient in those calculations adjusted to the OEC wavelengths of 467, 530, and 660 nm through log-interpolation. The data are from a high-loading kerosene soot aerosol run, and show $\sigma_{ap} \approx C\lambda^{-0.99}$, where C = a fitting constant and λ = wavelength. The other RAOS kerosene soot runs also showed very similar wavelength dependence of $\sigma_{ep} - \sigma_{sp}$ (i.e., $\lambda^{-0.94} - \lambda^{-1.0}$). A number of other investigators have found a spectral dependence in the visible range for atmospheric aerosol absorption measurements very close to λ^{-1} (e.g., Bruce et al. 1991 ($\sim \lambda^{-1}$); Horvath et al. 1997 ($\lambda^{-0.92}$); Bergstrom et al. 2002 ($\sim \lambda^{-1}$); T. W. Kirchstetter, personal communication 2003 ($\sim \lambda^{-1}$)). These results support the observations of many investigators of atmospheric BC and suggest that the small particle limit of λ^{-1} is at times applicable when estimating the wavelength dependence of atmospheric aerosol light absorption. In this study, all wavelength adjustments have been performed using a λ^{-1} wavelength dependence.

In one RAOS all-kerosene soot test run, very high concentrations of kerosene soot were stably produced and sampled. The mass determinations from this run were used to calculate the light-absorption efficiency (α_{ap}) of fine kerosene soot particles. Other lower-loading kerosene soot aerosol tests were not used because the lower mass measurements on filters were less certain due to blank subtraction issues and artifacts other than

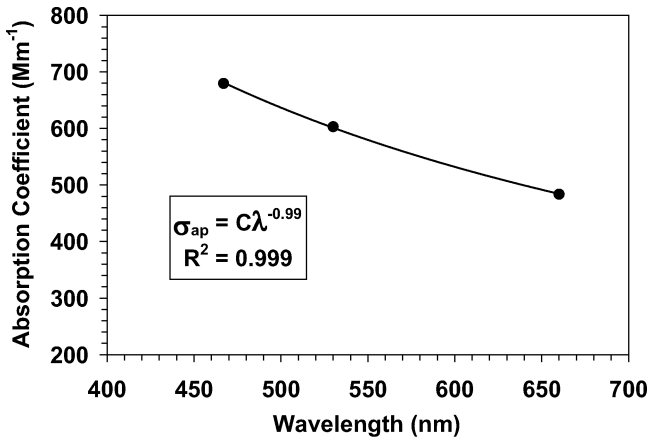

Figure 7. Wavelength dependence of the absorption coefficient measured during a typical kerosene soot run as determined by the "extinction minus scattering" method. Other runs on kerosene soot aerosols showed a similar wavelength dependence in the $\lambda^{-0.94} - \lambda^{-1.0}$ range.

the higher mass values. For this test, the EC concentration (as determined using the methods of Chow et al. 1993) was 78.9 μg m^{-3}. The determination of EC is complicated because more than one major thermal evolution protocol is commonly in use, and EC measurements using these two protocols have shown considerable disagreement (Chow et al. 2001; Schmid et al. 2001).

The total aerosol mass concentration during this sampling period determined from gravimetric analysis of a teflon filter was 80.1 ± 6.7 μg m^{-3} (reported uncertainty is the errors associated with the balance, filter handling, and flow measurement added in quadrature), while the TEOM aerosol mass concentration was 87.1 μg m^{-3}. We believe the reported TEOM mass concentration may be influenced by several apparent spikes during the test, which were probably caused by minor sample line pressure or RH fluctuations. The TEOM is sensitive to these artifacts and reports pressure and RH changes at the filter as mass changes. This is another reason why lower-concentration runs were not considered for this α_{ap} calculation; these TEOM artifacts become responsible for an increasingly large fraction of the reported mass at lower aerosol mass concentrations. The $\sigma_{ap(REF)}$ for this run was determined to be 599 ± 86 Mm^{-1}. The total uncertainty was calculated from the uncertainties of the photoacoustic (±5%, Arnott et al. 2000), the TSI nephelometer (±9%, Sheridan et al. 2002; Masonis et al. 2002), and the OEC (±10%) measurements. For the OEC, it was difficult to estimate the absolute uncertainty because its accuracy was assessed relative to a TSI nephelometer measuring nonabsorbing aerosols (Virkkula et al. 2005a). For the 10 reported runs in Virkkula et al. (2005a), which did not include the high-absorption run we are describing, measurement accuracy varied from ~1% to ~10% with the precision typically better. We have taken the average measurement accuracy of these runs and propagated the uncertainty of the TSI nephelometer into our OEC uncertainty determination. The uncertainties of ($\sigma_{ep} - \sigma_{sp}$) and σ_{ap} (photoacoustic) were then added in quadrature to arrive at the total $\sigma_{ap(REF)}$ uncertainty. Using 80.1 ± 6.7 μg m^{-3} for the EC mass and 599 ± 86 Mm^{-1} for the $\sigma_{ap(REF)}$ for this run, the α_{ap} was determined to be 7.5 ± 1.2 m^2 g^{-1}.

The other black aerosol used in this study, mechanically generated graphite particles, had very different wavelength dependencies for the few graphite runs we made. This is probably due to the fact that the graphite existed predominantly as irregularly shaped larger particles ($D_p > 0.5$ μm), and variability of the passing efficiency through the sampling lines and instruments for a few larger particles in the 0.5–0.75 um diameter range could influence the determined wavelength dependence greatly.

As discussed above, our two most fundamental independent methods for determining aerosol light absorption were photoacoustic spectroscopy and the difference between suspended-state aerosol extinction and scattering. The agreement between photoacoustic and ($\sigma_{ep} - \sigma_{sp}$) absorption on externally mixed kerosene soot and ammonium sulfate aerosols is shown in Figure 8a. In this comparison, the photoacoustic absorption measurements were adjusted from 532 nm to the OEC wavelengths using a λ^{-1} wavelength dependence. Thus, only the 530 nm comparison represents a comparison between truly independent methods, while the 467 and 660 nm comparisons rely on the applicability of the assumed λ^{-1} wavelength dependence for absorption.

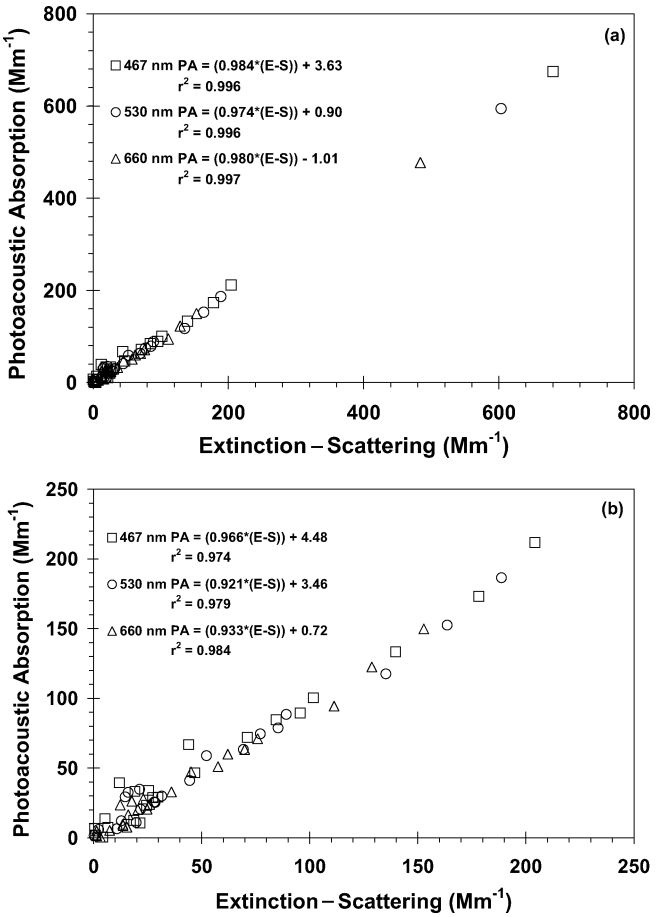

Figure 8. (a) Aerosol light absorption measured by the DRI photoacoustic instrument plotted against the difference of extinction and scattering. (b) If the high absorption run from Figure 8a is excluded, the regression slopes change.

A wide range of absorption values was used for this comparison. Since one purpose of this experiment was to characterize instruments for ambient aerosol light absorption, most of the tests were conducted at σ_{ap} levels well below 100 Mm^{-1}. A limited number of runs were conducted between 100 and 200 Mm^{-1}, and one high absorption, all-soot run was conducted. Since this high absorption data point can strongly influence the regression slopes and is not representative of typical atmospheric absorption levels, we recalculated the regression lines excluding this data point. The results are shown in Figure 8b. The slopes are different when the high absorption point is excluded, suggesting some nonlinearity in the relationship at

higher absorption levels. Still, considering that the slopes are <1.0 with small positive offsets, the agreement between the two methods is within ~3–7% over all three wavelengths, which suggests not only that these two methods show good agreement in their determination of the absorption coefficient but also that the λ^{-1} wavelength dependence for absorption used in this study is appropriate.

The primary instrument used for routinely measuring in situ aerosol light absorption in both the NOAA/CMDL network of surface aerosol monitoring stations and the DOE/ARM program is a PSAP. This instrument is a filter-based method that measures the incremental attenuation of light by aerosol particles that are being deposited continuously on the filter. The response of the PSAP has been calibrated by the work of B1999, which determined the factors necessary to correct for the multiple scattering filter medium and for the presence of scattering particles on the filter surface. The B1999 correction scheme also adjusts the wavelength of the determined σ_{ap} to 550 nm. The B1999 study used a black nigrosin dye solution for nebulizing black aerosols in their study. This solution formed small spherical particles upon drying, rather than the chain aggregates of spherules commonly observed in atmospheric soots. The PSAP filter-loading correction function was also not empirically determined in B1999; rather, the manufacturer's loading correction function was investigated and found to be satisfactory. One of the major objectives of the RAOS was to determine whether the PSAP calibration methods of B1999 produced corrected PSAP data that agreed well with the RAOS reference absorption methods.

The PSAP calculates an absorption coefficient as shown in Equation (1):

$$\begin{aligned}\sigma_{\mathrm{PSAP}} &= f(Tr) * (A/Q\Delta t) * \ln\left[(\Sigma_{\mathrm{SIG}}/\Sigma_{\mathrm{REF}})_{t-\Delta t}\right. \\ &\quad \left./(\Sigma_{\mathrm{SIG}}/\Sigma_{\mathrm{REF}})_{t}\right] \\ &= f(Tr) * \sigma_{\mathrm{ap(raw)}}, \end{aligned} \quad [1]$$

where Tr is the filter transmittance, $f(Tr)$ is the loading correction function, A is the area of the aerosol deposit on the filter, Q is the calibrated flow rate, t is the current time, Δt is the integration period, and Σ_{SIG} and Σ_{REF} are the average sample and reference detector signal intensities, respectively, over the integration period. The quantity $\sigma_{\mathrm{ap(raw)}}$ is the absorption coefficient computed by the PSAP without any loading correction applied. The σ_{PSAP} includes an empirical correction for multiple scattering in the filter matrix, but not for scattering particles on the filter surface. The value of $f(Tr)$ used in B1999 was

$$f(Tr) = 0.873/(1.0796 * Tr + 0.71), \quad [2]$$

with the only difference between this function and that originally proposed by the manufacturer being the factor of 0.873, which is the ratio of aerosol spot areas used (1.783e-5 m^2 assumed by the manufacturer and 2.043e-5 m^2 in the actual instrument used in the manufacturer's calibration tests).

The PSAP light source/detector system was postcalibrated using a spectrophotometer (D. S. Covert, personal communication 2002) and was found to operate at a slightly different wavelength (574 nm) than that quoted by the manufacturer (565 nm). A detailed analysis of the RAOS PSAP data, which take into account this wavelength difference and include a newly derived loading correction function and filter/aerosol scattering corrections, is described in Virkkula et al. (2005b). The analysis of Virkkula et al. (2005b) shows that the existing B1999 loading correction function agrees closely with that expected from the RAOS data for filter transmittances (Tr) > ~0.8 ($Tr = 1.0$ for a new filter). Below $Tr = 0.8$, the B1999 and Virkkula et al. (2005b) $f(Tr)$'s diverge and at $Tr = 0.7$ differ by ~15%. The B1999 PSAP correction scheme was not tested for $Tr < 0.7$, so its validity at lower Tr values is unknown (B1999). Most aerosol tests in the RAOS were conducted with PSAP filter transmittances >0.7, so the B1999 PSAP corrections are applied here for comparison of PSAP absorption to other RAOS absorption methods.

Figure 9a shows PSAP 550 nm absorption coefficients (adjusted to 530 nm using a λ^{-1} wavelength dependence) plotted

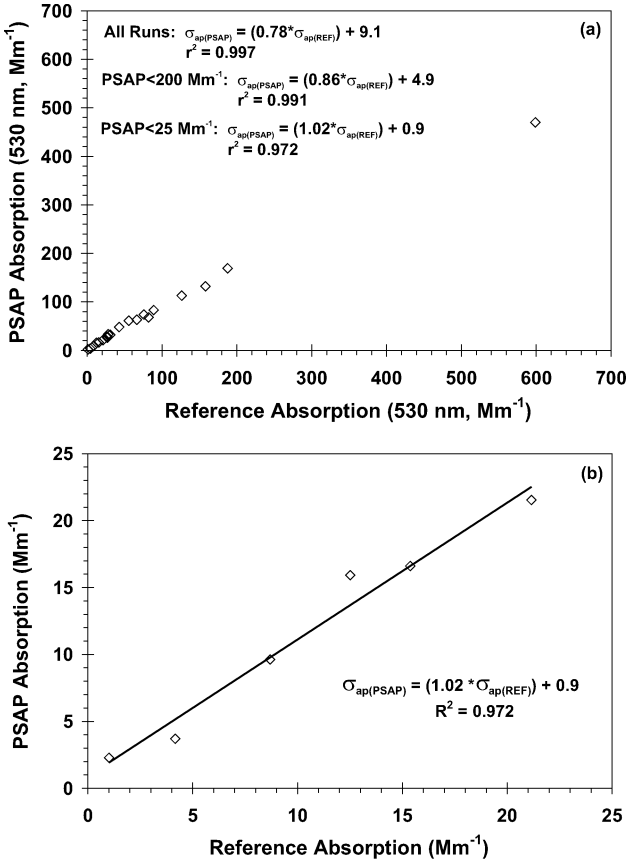

Figure 9. (a) Linear regression fits of the mixed kerosene soot/ammonium sulfate aerosol absorption data (530 nm) over several ranges. (b) Linear fit of the absorption data in the atmospherically relevant ($\sigma_{ap} < 25$ Mm^{-1}) range.

against the 530 nm reference σ_{ap} values for all valid mixed kerosene soot/ammonium sulfate aerosol runs. If all runs are considered, the slope of the linear regression fit of the data is ~0.78. If the one high absorption case that heavily weights the fit is excluded, all PSAP absorption coefficients are <200 Mm^{-1} and the slope of the regression line changes to ~0.86. If we only consider absorption levels with typical atmospheric relevance (e.g., σ_{ap} <25 Mm^{-1}), the regression slope changes to ~1.02, although there is considerable spread in the data around the regression line. Figure 9b shows only the low absorption data. One test run was eliminated from this analysis as a statistical outlier; this experiment was conducted on DOY 177, and the suspect runs from this day have been discussed by Virkkula et al. (2005a). The slope and intercept suggest an agreement between these two absorption methods of within 3%, but two points must be made at this time in describing this agreement. First, the favorable comparison between the absorption methods was probably influenced by the controlled set of laboratory conditions under which the tests were conducted. Relative humidities in the aerosol delivery system were kept low (<25%) and consistent over the course of a test run or subrun. Aerosol mixtures were also kept as stable as possible, and these were typically binary external mixtures of black and white aerosols. Rapid changes in aerosol concentrations and compositions were avoided, thereby minimizing differences between methods with different time constants, residence times, or sensitivities to moisture. For these reasons, it is quite possible that agreement between these absorption methods in the field using atmospheric aerosols might not be as impressive. Second, it must be noted that in this comparison there is considerable variability in the data in this low absorption range. Calculation of $(\sigma_{ap(PSAP)} - \sigma_{ap(REF)})/\sigma_{ap(REF)})$ shows that four of the six values were <~11%, although the one lowest absorption point shows a value larger than 100%. This sample-to-sample variability is probably due to increased noise in both the PSAP and $(\sigma_{ep} - \sigma_{sp})$ absorption determination at the lowest absorption values. Clearly, the absorption data from these two instruments do not display a linear relationship over the entire measurement range; the reason for this may be an inadequate B1999 correction at high absorption levels where the *Tr* often dropped below 0.7. In some cases we let the aerosol test runs continue until the PSAP *Tr* reached 0.5, which is the limit stated by the manufacturer. This is not to suggest that the B1999 corrections are appropriate in the $0.5 < Tr < 0.7$ region, but simply to show what happens here. This was done because a possible outcome of this work was to develop a new PSAP correction function, and we needed to enter the $Tr < 0.7$ range to determine the new corrections (Virkkula et al. 2005b).

These data suggest that the B1999 correction scheme (including the manufacturer's loading correction function, which was found in B1999 to be satisfactory) overcorrects the PSAP data at high absorption levels. It is not clear whether this overcorrection is the result of an inadequate $f(Tr)$ or that the simple filter/aerosol scattering corrections developed in B1999 may not be representative of the aerosols generated in this study for all absorption and aerosol levels. The agreement at atmospherically relevant absorption levels between the B1999-corrected PSAP and reference absorption measurements of low RH, externally mixed aerosols is very good. Thus, for atmospheric aerosol scenarios that are not dominated by high concentrations of absorbing aerosols or proximity of combustion sources, the filter-based PSAP absorption measurement is a reasonable surrogate for either a photoacoustic absorption measurement or an extinction-minus-scattering measurement system.

The higher absorption aerosol test runs in RAOS, where the $\sigma_{ap(PSAP)}/\sigma_{ap(REF)}$ ratio was usually farthest from unity, typically exhibited lower final PSAP *Tr* and lower ϖ_0 than the lower absorption runs, and they are the cases where the potential overcorrection needs to be explained. In Figure 10, four similar RAOS aerosol runs are presented that show different behavior of the PSAP absorption coefficient (corrected using B1999 methods and adjusted to 532 nm) relative to the concurrent 532 nm photoacoustic absorption measurement over time. In each plot the *x* axis is run time in minutes and the data points represent 1 min averages of the plotted parameters. The photoacoustic absorption is presented here rather than the reference absorption because the $(\sigma_{ep} - \sigma_{sp})$ absorption measurement was often switched into a zero mode just prior to when the PSAP *Tr* approached 0.5. For this study we used the high-extinction target runs (σ_{ep} = 500–800 Mm^{-1}); these should have less measurement noise than the lighter loading runs. All four absorption time series show the PSAP *Tr* starting at or very near 1.0 and ending near 0.5. The only major differences between the four runs are the composition of the aerosol (i.e., the white/black aerosol mix) and the time required for the *Tr* to drop to 0.5. In Figure 10a, the aerosol is all kerosene soot, with a ϖ_0 of ~0.3 (as calculated from the 532 nm DRI integrating sphere nephelometer σ_{sp} and DRI photoacoustic σ_{ap} measurements). Figures 10b, 10c, and 10d show aerosol data from progressively higher ϖ_0 (i.e., higher ratio of $(NH_4)_2SO_4$ to kerosene soot) cases. In Figure 10a, a divergence between fully corrected PSAP absorption and photoacoustic absorption is evident from the very beginning of the run. At $Tr = 0.7$, the point above which the B1999 corrections for the PSAP are presumed valid, the PSAP σ_{ap} has dropped to ~470 Mm^{-1} while the photoacoustic σ_{ap} has remained steady at ~600 Mm^{-1}. The average value of the corrected PSAP σ_{ap} over this interval is ~540 Mm^{-1}, compared with the photoacoustic σ_{ap} of ~600 Mm^{-1}. By $Tr =$ 0.5, the corrected PSAP σ_{ap} is near 400 Mm^{-1}. The decrease in the B1999-corrected PSAP σ_{ap} with time is the effect which caused the high-absorption, run-averaged data point in Figure 9 to lie far below where a 1:1 line would pass. As the aerosol gets lighter (i.e., increasing ϖ_0), the divergence between the two traces tends to decrease. A significant effect is still observed at $\varpi_0 = 0.67$ (Figure 10b), where the PSAP σ_{ap} starts above and ends up far below the photoacoustic σ_{ap}. Figure 10c shows that at $\varpi_0 = 0.78$, only a small effect is seen, and at $\varpi_0 = 0.88$ (Figure 10d) essentially no decrease in the PSAP σ_{ap} relative to the photoacoustic σ_{ap} can be observed. In these high-loading

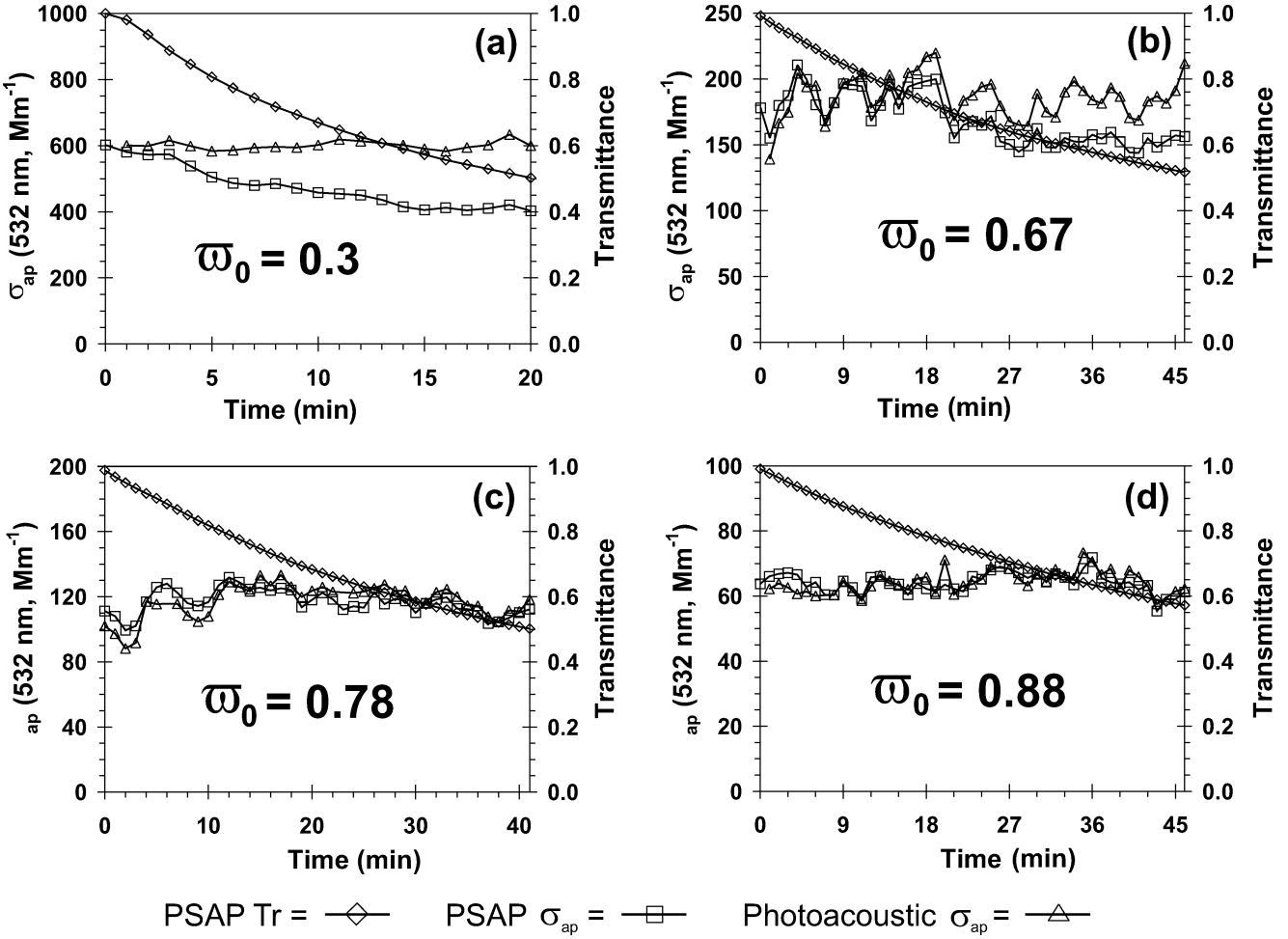

Figure 10. Time series of 1 min average absorption data from the PSAP and photoacoustic instruments. The divergence between the corrected PSAP σ_{ap}, and the photoacoustic σ_{ap} is greatest at lower ϖ_0.

cases, the critical ϖ_0 above which no divergence effect was observed was in the 0.80–0.85 range. These data suggest that for these aerosols and loadings, the manufacturer's loading correction for the PSAP needs to account in some way for scattering rather than be simply a function of *Tr*. The parameterization could possibly include either σ_{sp} or ϖ_0. A proper scattering correction should probably not merely be a percentage of scattering to be subtracted from absorption but a variable amount that depends on the filter transmittance and ϖ_0 (Virkkula et al. 2005b).

Assuming that the aerosol mixtures we generated and tested can be representative of ambient atmospheric aerosols, these observations suggest that PSAP absorption measurements of dark, highly absorbing atmospheric aerosols are the most likely to be in error using the B1999 correction scheme. Most atmospheric aerosols have a $\varpi_0 > 0.75$, and the divergence effect is relatively small in this range. Care should be taken when using the B1999-corrected PSAP method to determine the absorption coefficient of urban pollution, vehicular emissions, biomass burning plumes, or other aerosols with a significant combustion component.

In Figure 11, the run average values of σ_{ap} for the MAAP are plotted against those from the reference absorption method. The MAAP σ_{ap} values were adjusted from 670 to 660 nm using a λ^{-1} wavelength adjustment. The plotted data points represent all runs where the aerosols were either pure kerosene soot or mixed kerosene soot and ammonium sulfate, and the extinction coefficient from the OEC was >50 Mm^{-1}. Unlike the PSAP data, the MAAP data show a strong linear relationship with the reference absorption over an extended σ_{ap} range (approaching 500 Mm^{-1}) and a linear regression slope of 0.99. If we disregard the one high absorption run that heavily influences the fit, the slope, offset, and correlation coefficient change to 1.04, 1.0, and 0.99, respectively, for all run-average data between 0 and ~150 Mm^{-1}. It appears from these data that the angular-resolved detection of backscattered radiation from the front side of the filter provides additional information on the light-scattering fraction of the deposited aerosol and that information of this type may help

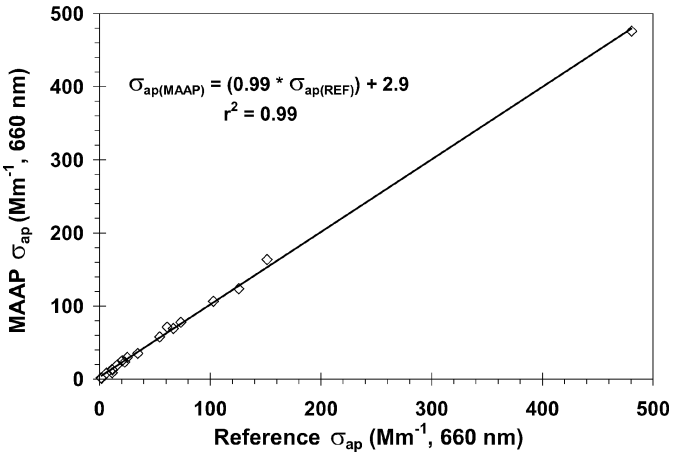

Figure 11. Run-averaged light-absorption coefficient from the MAAP instrument plotted against the reference absorption. MAAP absorption has been adjusted to 660 nm using a λ^{-1} wavelength dependence. If the high absorption run is ignored, the linear regression slope changes to 1.04 over the σ_{ap} range 0–160 Mm^{-1}.

to reduce the cross-sensitivity of filter-based absorption measurement methods to light-scattering aerosol components and filter-loading effects.

Run-averaged aerosol extinction coefficients measured by the three CRD instruments were compared with the sum of nephelometer scattering and PSAP absorption measurements. These comparisons indicated that all of the CRD instruments systematically measured extinction coefficients 8–13% less than that sum. As was noted above, great care was taken to ensure that all of the instruments sampled the same aerosol. Thus it is puzzling that all three of the CRD measurements, employing different measurement strategies, were systematically low. Pulsed CRD measurements (PSU CRD instrument) of the extinction of the common span gas HFC-134a in the visible (532 nm) agreed with published scattering cross sections to within 2%. Experiments, performed at NASA American Research Center prior and subsequent to RAOS, showed good agreement between Cadenza extinction measurements of polystyrene latex (PSL) calibration spheres and Mie theory predictions of extinction (Strawa et al. 2003). Comparisons between Cadenza extinction measurements and nephelometer + PSAP extinction made during an intensive DOE aerosol field experiment showed better agreement than observed in RAOS (Schmid et al. 2003; Strawa et al., 2005). Some aerosol plumbing issues were identified with the DRI CRD that contributed to uncertainty in the calibration of this instrument during RAOS. At this point the difference between the CRD and the nephelometer + PSAP measurements during RAOS remains unexplained. Due to the rapid pace of development and improvement in the CRD technique and instrumentation, we feel that it is not productive to further analyze the differences observed in RAOS.

SUMMARY

The RAOS was conducted in June 2002 to compare the performance of existing and new instruments for the measurement of in situ aerosol optical properties, with an emphasis on the light-absorption measurement. Test aerosols of absorbing and nonabsorbing (black and white) particles were generated, mixed, and delivered as predominantly external mixtures to each instrument in the study. A large, stirred mixing chamber with baffles ensured a well-mixed aerosol, and a number of characterization measurements of the aerosol microphysical and chemical properties were made at various points in the system to verify that essentially identical aerosols were being sampled by each instrument. The majority of the test aerosols were mixtures of kerosene soot and ammonium sulfate, and all tests were done at low RH (usually between 15–25%).

The extinction measurements from a folded-path optical extinction cell were compared with the scattering measurements from a TSI integrating nephelometer on nonabsorbing ammonium sulfate aerosols and were found to agree closely after the scattering measurements were corrected for truncation effects and other angular nonidealities. The difference in these measurements was $<1\%$ at the blue and green wavelengths, and $\sim 2\%$ for the red wavelength.

The wavelength dependence of absorption was investigated for all three types of absorbing particles. For the kerosene and diesel soots, measurements from most instruments showed a wavelength dependence near λ^{-1}, the theoretical small-particle limit. The large, irregularly shaped graphite particles showed widely variable wavelength dependencies over several graphite runs. This could be due to changing size distributions of the graphite related to sample line passing efficiency issues or an unsteady source of the particles. The light-absorption efficiency at a wavelength of 530 nm for pure kerosene soot with a number size distribution peak near 0.3 μm diameter was found to be 7.5 ± 1.2 m^2 g^{-1}.

The two most fundamental independent absorption methods used in this study, photoacoustic absorption and the difference between suspended-state extinction and scattering, also showed excellent agreement on mixed black/white aerosols. If all stable mixed kerosene soot and ammonium sulfate runs are considered, the agreement is within a few percent (with the photoacoustic absorption slightly lower) for absorption levels in the visible wavelength region up to ~ 800 Mm^{-1}. If the one high absorption run is excluded, the difference in the two sets of measurements increases to ~ 3–7%, depending on wavelength. The average of these two measurements was taken as the reference absorption.

Excellent agreement was observed between the filter-based PSAP absorption and the reference absorption for typical atmospherically relevant levels of the light absorption coefficient under the controlled laboratory conditions of our comparison tests. It is not clear that similar agreement should be expected from ambient atmospheric aerosols where changes in aerosol composition, concentration, and RH could negatively impact the comparisons. For test aerosols exhibiting higher absorption

(and a lower single-scattering albedo), the agreement between the methods worsened with decreasing ϖ_0, presumably because of an inadequate filter loading correction. The Bond et al. (1999) correction scheme appears to do a good job of correcting the PSAP absorption in our aerosol mixtures at $\varpi_0 > 0.80$–0.85, which represents most atmospheric aerosols. For the aerosol runs considered in this study, most of which had at least some periods where PSAP filter transmission was below 0.8, the Bond et al. (1999) corrections did a reasonable job of correcting the PSAP data so that it closely agreed with the reference absorption methods. At higher aerosol absorption levels (which in this study were characterized by aerosol runs where the ϖ_0 was typically lower than 0.8), the Bond et al. (1999) corrected PSAP absorption data showed a less favorable agreement with RAOS reference absorption measurements, presumably because of the existing PSAP filter-loading correction. The work of Virkkula et al. (2004b) has produced a new empirical PSAP loading correction function from the RAOS data that appears to work better at lower filter transmission values.

A new filter-based light-absorption instrument called MAAP was also evaluated in RAOS. The MAAP detects light scattered from the front of the filter and aerosol deposit along with that transmitted through the filter. It uses a two-stream radiative transfer model to better determine the filter and aerosol scattering effects for its calculation of the absorption coefficient. The MAAP absorption values agreed with the reference absorption closely (linear regression slope of $\sim$0.99) for all experiment tests on externally mixed kerosene soot and ammonium sulfate.

REFERENCES

Ackerman, T. P., and Toon, O. B. (1981). Absorption of Visible Radiation in Atmospheres Containing Mixtures of Absorbing and Nonabsorbing Aerosols, *Appl. Opt.* 20:3661–3667.

Anderson, T. L., and Ogren, J. A. (1998). Determining Aerosol Radiative Properties Using the TSI 3563 Integrating Nephelometer, *Aerosol Sci. Technol.* 29:57–69.

Andreae, M. O. (2001). The Dark Side of Aerosols, *Nature* 409:671–672.

Ansmann, A., Wandinger, U., Wiedensohler, A., and Leiterer, U. (2002). Lindenberg Aerosol Characterization Experiment 1998 (LACE 98): Overview, *J. Geophys. Res.* 107(D21):8129.

Arnott, W. P., Moosmüller, H., and Walker, J. W. (2000). Nitrogen Dioxide and Kerosene-Flame Soot Calibration of Photoacoustic Instruments for Measurement of Light Absorption by Aerosols, *Rev. Sci. Inst.* 71(7):4545–4552.

Arnott, W. P., Hamasha, K., Moosmüller, H., Sheridan, P. J., and Ogren, J. A. (2005). Towards Aerosol Light Absorption Measurements with a Seven-Wavelength Aethalometer: Evaluation with a Photoacoustic Instrument and Three-Wavelength Nephelometer, *Aerosol Sci. Technol.* 39:17–29.

Bergstrom, R. W. (1973). Extinction and Absorption Coefficients of the Atmospheric Aerosol as a Function of Particle Size, *Beitr. Phys. Atmos.* 46:223–234.

Bergstrom, R. W., Russell, P. B., and Hignett, P. (2002). Wavelength Dependence of the Absorption of Black Carbon Particles: Predictions and Results from the TARFOX Experiment and Implications for the Aerosol Single Scattering Albedo, *J. Atmos. Sci.* 59:567–577.

Bohren, C. F., and Huffman, D. R. (1983). *Absorption and Scattering of Light by Small Particles*. John Wiley and Sons, New York.

Bond, T. C., Anderson, T. L., and Campbell, D. (1999). Calibration and Intercomparison of Filter-Based Measurements of Visible Light Absorption by Aerosols, *Aerosol Sci. Technol.* 30:582–600.

Bruce, C. W., Stromberg, T. F., Gurton, K. P., and Mozer, J. B. (1991). Trans-Spectral Absorption and Scattering of Electromagnetic Radiation by Diesel Soot, *Appl. Opt.* 30:1537–1546.

Charlson, R. J., Langner, J., Rodhe, H., Leovy, C. B., and Warren, S. G. (1991). Perturbation of the Northern Hemisphere Radiative Balance by Backscattering from Anthropogenic Sulfate Aerosols, *Tellus, Ser. A* 43:152–163.

Chow, J. C., Watson, J. G., Pritchett, L. C., Pierson, W. R., Frazier, C. A., and Purcell, R. G. (1993). The DRI Thermal/Optical Reflectance Carbon Analysis System: Description, Evaluation and Applications in U.S. Air Quality Studies, *Atmos. Environ.* 27A:1185–1201.

Chow, J. C., Watson, J. G., Crow, D., Lowenthal, D. H., and Merrifield, T. (2001). Comparison of IMPROVE and NIOSH Carbon Measurements, *Aerosol Sci. Technol.* 34:23–34.

Coakley, J. A., and Cess, R. D. (1985). Response of the NCAR Community Climate Model to the Radiative Forcing by the Naturally Occurring Tropospheric Aerosol, *J. Atmos. Sci.* 42:1677–1692.

Covert, D. S., Charlson, R. J., and Ahlquist, N. C. (1972). A Study of the Relationship of Chemical Composition and Humidity to Light Scattering by Aerosols, *J. Appl. Meteor.* 11:968–976.

Fuller, K. A., Malm, W. C., and Kreidenweis, S. M. (1999). Effects of Mixing on Extinction by Carbonaceous Particles, *J. Geophys. Res.* 104:15941–15954.

Gerber, H. E. (1982a). Absorption of Light by Atmospheric Aerosol Particles: Review of Instrumentation and Measurements. In *Light Absorption by Aerosol Particles*, edited by H. E. Gerber and E. E. Hindman, Technical Proceedings of the First International Workshop on Light Absorption by Aerosol Particles, Spectrum Press, Hampton, VA, pp. 21–43.

Gerber, H. E. (1982b). Optical Techniques for the Measurement of Light Absorption by Particulates. In *Particulate Carbon, Atmospheric Life Cycle*, edited by G. T. Wolff and R. Klimisch, Plenum Press, New York.

Hansen, J., Sato, M., and Ruedy, R. (1997). Radiative Forcing and Climate Response, *J. Geophys. Res.* 102:6831–6864.

Horvath, H. (1993). Atmospheric Light Absorption—A Review, *Atmos. Environ.* 27A:293–317.

Horvath, H., Catalan, L., and Trier, A. (1997). A Study of the Aerosol of Santiago de Chile III: Light Absorption Measurements, *Atmos. Environ.* 31:3737–3744.

Intergovernmental Panel on Climate Change (IPCC). (1995). *Climate Change 1994: Radiative Forcing of Climate,* Report to IPCC From the Scientific Assessment Group (WGI), Cambridge University Press, New York.

Intergovernmental Panel on Climate Change (IPCC). (2001). *Climate Change 2001: The Scientific Basis,* Contribution of Working Group I to the Third Assessment Report of the IPCC, Cambridge University Press, New York.

Kaufman, Y. J., Hobbs, P. V., Kirchhoff, V. W. J. H., Artaxo, P., Remer, L. A., Holben, B. N., King, M. D., Ward, D. E., Prins, E. M., Longo, K. M., Mattos, L. F., Nobre, C. A., Spinhirne, J. D., Ji, Q., Thompson, A. M., Gleason, J. F., Christopher, S. A., and Tsay, S.-C. (1998). Smoke, Clouds and Radiation-Brazil (SCAR-B) Experiment, *J. Geophys. Res.* 103(D24):31783–31808.

Kittleson, D. B. (1998). Engines and Nanoparticles: A Review, *J. Aerosol Sci.* 29:575–588.

Masonis, S. J., Franke, K., Ansmann, A., Müller, D., Althausen, D., Ogren, J. A., Jefferson, A., and Sheridan, P. J. (2002). An Intercomparison of Aerosol Light Extinction and 180° Backscatter as Derived Using in situ Instruments and Raman Lidar During the INDOEX Field Campaign, *J. Geophys. Res.* 107 (D19):8014.

Moosmüller, H., Varma, R., and Arnott, W. P. (2005). Cavity Ring-Down and Cavity-Enhanced Detection Techniques for the Measurement of Aerosol Extinction. *Aerosol Sci. Technol.* 39:30–39.

Panne, U., Petzold, A., and Niessner, R. (1995). Diesel Exhaust Particle Size Distribution Measurements under Dynamic Conditions, *J. Aerosol Sci.* 26:s659–s660.

Petzold, A., Fiebig, M., Flentje, H., Keil, A., Leiterer, U., Schröder, F., Stifter, A., Wendisch, M., and Wendling, P. (2002). Vertical Variability of Aerosol Properties Observed at a Continental Site During the Lindenberg Aerosol Characterization Experiment (LACE 98), *J. Geophys. Res.* 107(D21):8128.

Petzold, A., and Schönlinner, M. (2004). Multi-Angle Absorption Photometry—A New Method for the Measurement of Aerosol Light Absorption and Atmospheric Black Carbon, *J. Aerosol Sci.* 35:421–441.

Petzold, A., Schloesser, H., Sheridan, P. J., Arnott, W. P., Ogren, J. A., and Virkkula, A. (2005). Evaluation of Multi-Angle Absorption Photometry for Measuring Aerosol Light Absorption, *Aerosol Sci. Technol*. 39:40–51.

Ramanathan, V., Crutzen, P. J., Lelieveld, J., Mitra, A. P., Althausen, D., Anderson, J., Andreae, M. O., Cantrell, W., Cass, G. R., Chung, C. E., Clarke, A. D., Coakley, J. A., Collins, W. D., Conant, W. C., Dulac, F., Heintzenberg, J., Heymsfield, A. J., Holben, B., Howell, S., Hudson, J., Jayaraman, A., Kiehl, J. T., Krishnamurti, T. N., Lubin, D., McFarquhar, G., Novakov, T., Ogren, J. A., Podgorny, I. A., Prather, K., Priestley, K., Prospero, J. M., Quinn, P. K., Rajeev, K., Rasch, P., Rupert, S., Sadourny, R., Satheesh, S. K., Shaw, G. E., Sheridan, P., and Valero, F. P. J. (2001). Indian Ocean Experiment: An Integrated Analysis of the Climate Forcing and Effects of the Great Indo-Asian Haze, *J. Geophys. Res.* 106:28371–28398.

Redemann, J., Russell, P. B., and Hamill, P. (2001). Dependence of Aerosol Light Absorption and Single-Scattering Albedo on Ambient Relative Humidity for Sulfate Aerosols with Black Carbon Cores, *J. Geophys. Res.* 106:27485–27495.

Rood, M. J., Covert, D. S., and Larson, T. V. (1987). Hygroscopic Properties of Atmospheric Aerosol in Riverside, California, *Tellus* 39B:383–397.

Rosenfeld, D. (2000). Suppression of Rain and Snow by Urban and Industrial Air Pollution, *Science* 287:1793–1796.

Russell, P. B., Livingston, J. M., Hignett, P., Kinne, S., Wong, J., Chien, A., Bergstrom, R., Durkee, P., and Hobbs, P. V. (1999). Aerosol-Induced Radiative Flux Changes off the United States Mid-Atlantic Coast: Comparison of Values Calculated from Sunphotometer and in situ Data with Those Measured by Airborne Pyranometer, *J. Geophys. Res.* 104:2289–2307.

Saathoff, H., Moehler, O., Schurath, U., Kamm, S., Dippel, B., and Mihelcic, D. (2003a). The AIDA Soot Aerosol Characterisation Campaign 1999, *J. Aerosol. Sci.* 34:1277–1296.

Saathoff, H., Naumann, K.-H., Schnaiter, M., Schöck, W., Möhler, O., Schurath, U., Weingartner, E., Gysel, M., and Baltensperger, U. (2003b). Coating of Soot and $(NH_4)_2SO_4$ Particles by Ozonolysis Products of α-Pinene, *J. Aerosol Sci.* 34:1297–1321.

Schmid, B., Arnott, W., Bucholtz, A., Colarco, P., Covert, D., Eilers, J., Elleman, R., Ferrare, R., Flagan, R., Jonsson, H., Pilewskie, P., Pommier, J., Redemann, J., Ricci, K., Rissman, T., Seinfeld, J., Strawa, A., VanReken, T., Wang, J., and Welton, E. (2003). Measurement and Modeling of Vertically Resolved Aerosol Optical Properties and Radiative Fluxes Over the ARM SGP Site, *EOS Trans. AGU* 84(46): Fall Meet. Suppl., Abstract A21G-06.

Schmid, H., Laskus, L., Abraham, H. J., Baltensperger, U., Lavanchy, V., Bizjak, M., Burba, P., Cachier, H., Crow, D., Chow, J., Gnauk, T., Even, A., ten Brink, H. M., Giesen, K.-P., Hitzenberger, R., Hueglin, C., Maenhaut, W., Pio, C., Carvalho, A., Putaud, J.-P., Toom-Sauntry, D., and Puxbaum, H. (2001). Results of the "Carbon Conference" International Aerosol Carbon Round Robin Test Stage I, *Atmos. Environ.* 35:2111–2121.

Sheridan, P. J., Jefferson, A., and Ogren, J. A. (2002). Spatial Variability of Submicrometer Aerosol Radiative Properties over the Indian Ocean during INDOEX, *J. Geophys. Res.* 107(D19):8011.

Smith, J. D., and Atkinson, D. B. (2001). A Portable Pulsed Cavity Ring-Down Transmissometer for Measurement of the Optical Extinction of the Atmospheric Aerosol, *Analyst* 126:1216–1220.

Strawa, A. W., Castaneda, R., Owano, T., Baer, D. S., and Paldus, B. A. (2003). The Measurement of Aerosol Optical Properties Using Continuous Wave Cavity Ring-Down Techniques, *J. Atmos. Oceanic Technol.* 20:454–465.

Toon, O. B., Pollack, J. B., and Khare, B. N. (1976). The Optical Constants of Several Atmospheric Aerosol Species: Ammonium Sulfate, Aluminum Oxide, and Sodium Chloride, *J. Geophys. Res.* 81:5733–5748.

van de Hulst, H. C. (1957). *Light Scattering by Small Particles*, John Wiley and Sons, New York.

Varma, R., Moosmüller, H., and Arnott, W. P. (2003). Toward an Ideal Integrating Nephelometer, *Opt. Lett.* 28(12):1007–1009.

Virkkula, A., Ahlquist, N. C., Covert, D. S., Sheridan, P. J., Arnott, W. P., and Ogren, J. A. (2005a). A Three-Wavelength Optical Extinction Cell for Measuring Aerosol Light Extinction and Its Application to Determining Light Absorption Coefficient, *Aerosol Sci. Technol.* 39:52–67.

Virkkula, A., Ahlquist, N. C., Covert, D. S., Arnott, W. P., Sheridan, P. J., Quinn, P. K., and Coffman, D. J. (2005b). Modification, Calibration and a Field Test of an Instrument for Measuring Light Absorption by Particles, *Aerosol Sci. Technol.* 39:68–83.